

Development of Polarizable Water Force Fields for Phase Equilibrium Calculations

Bin Chen, Jianhua Xing,[†] and J. Ilja Siepmann*

Department of Chemistry and Department of Chemical Engineering and Materials Science, University of Minnesota, 207 Pleasant St. SE, Minneapolis, Minnesota 55455-0431

Received: October 15, 1999

Recent simulation studies for four dipole-polarizable and for two fluctuating-charge water force fields have demonstrated that none of the force fields studied is capable of yielding a satisfactory description of the vapor–liquid coexistence curve from room temperature to the critical region. The performance of these polarizable force fields can be improved dramatically by introducing an additional coupling between the Lennard–Jones interaction parameters for a pair of oxygen sites and their partial charges (electronic configuration). Two different types of water models are presented which are based on either the three-site simple point charge (SPC) or the four-site transferable intermolecular potential 4 point (TIP4P) water representations. Adiabatic nuclear and electronic sampling Monte Carlo (ANES-MC) simulations in the Gibbs, isobaric–isothermal, and canonical ensembles were performed to calculate vapor–liquid coexistence curves, to determine the temperatures of maximum liquid density, and to evaluate dielectric constants along the coexistence line, respectively. The new SPC-pol-1 force field yields significantly better agreement with the experiment for the saturated vapor and liquid densities, the heats of vaporization, and the liquid-phase dielectric constants than the fixed-charge SPC, SPC/E (simple point charge/extended), TIP4P, and Errington/Panagiotopoulos (EP) force fields or than any other polarizable force field previously tested. However, the representation of the liquid water structure at ambient conditions is less satisfactory for the SPC-pol force fields. In contrast, the TIP4P-pol force fields produce much better low-temperature liquid structures and, in particular, a density maximum close to $T = 277$ K, but their performance for the vapor–liquid equilibria in the near-critical region is less satisfactory. Finally, it is important to note that the SPC-pol-1 force field yields an average molecular dipole moment of 2.5 D for the liquid phase at ambient conditions that is substantially smaller than the value of 2.7 D obtained for its minimum-energy hexamer cluster.

1. Introduction

Both experimental and computational studies for water from small clusters to bulk phases emphasize one of the most important features of the aqueous systems: the strong many-body polarization effects.^{1–3} Nonpolarizable force fields, such as SPC,⁴ SPC/E,⁵ and TIP4P,⁶ use fixed electronic configurations which approximate the many-body effects at a certain thermodynamic state (usually liquid at ambient conditions) in a mean field way. These force fields are computationally very efficient, are very robust, and have been instrumental for advancing the field of biomolecular simulations. However, these fixed-charge force fields have limited transferability to other thermodynamic states and can exhibit problems in mixtures with ions or with nonpolar species, because the electronic configuration of a given water molecule should depend explicitly on its environment through the electronic many-body effect. For example, an isolated water molecule (in the gas phase) has a dipole moment of approximately 1.85 D,^{1,7,8} whereas the average dipole moment in a water dimer increases to 2.1 D.¹ There is considerable controversy on the exact value of the average molecular dipole moment in condensed phases. The most commonly accepted values for liquid water and ice are approximately 2.5 D^{9–11} and 2.6 D,¹² respectively, but recently values at about 3.0 D have been reported for liquid and solid phases.^{13–16} Thus for a

transferable water model that should yield satisfactory results for a wide range of thermodynamic states or environments of different polarity, it is essential to incorporate an explicit modeling of the electronic structure which allows for a qualitative (or better quantitative) description of the many-body response to environmental changes. Such force fields, which are called polarizable force fields, are computationally more expensive than fixed-charged force fields. However, empowered by novel simulation algorithms and steady increases in the computational resources, modeling of water using polarizable force fields has become a flourishing area in recent years.^{11,17–31}

Polarizable force fields can be divided into two main categories: dipole-polarizable and fluctuating-charge force fields. In dipole-polarizable force fields, polarizable dipoles centered (usually) on atomic sites are introduced to describe the induction effect (one of the major many-body effects) as follows

$$\mathbf{q}_i = \alpha_i \mathbf{E}_i \quad (1)$$

where \mathbf{q}_i is the induced dipole moment, α_i is the dipolar polarizability, and \mathbf{E}_i is the electric field, which includes contributions from all the molecules in the system. Equation 1 is usually solved self-consistently via an iterative procedure. The fluctuating-charge force fields are based on the electronegativity equalization (EE) method.^{24,28,32–34} Electronegativity is defined here as the negative of the gradient of the energy with respect to the electronic density, or as the negative of the chemical potential of the electron gas surrounding its nucleus.³³

[†] Present address: Department of Chemistry, University of California, Berkeley, CA 94720-1460.

* Corresponding author: siepmann@chem.umn.edu.

In a many-atom system, the electron gas will equilibrate with the instantaneous positions of the nuclei so that the electrochemical potentials of the electron gas will be equal at all fluctuating-charge sites. In the EE method, the molecular energy is approximated as a second-order Taylor expansion about the neutral atoms³⁴ (or molecular ground state, see ref 28) such that

$$E(\mathbf{Q}, \mathbf{R}) = \sum_{i=1}^N \left[E_i(0) + \chi_i Q_i + \frac{1}{2} J_{ii} Q_i^2 \right] + \sum_{i < j} J_{ij}(r_{ij}) Q_i Q_j \quad (2)$$

where $E(\mathbf{Q}, \mathbf{R})$ is the molecular energy of a configuration given by a set of electronic coordinates (\mathbf{Q}) and nuclear coordinates (\mathbf{R}), and $E_i(0)$ is the ground-state energy of atom i . The variables χ_i and J_{ii} are the Mulliken electronegativity and hardness of the isolated atom. The cross-parameter J_{ij} is the Coulombic interaction between unit charges on atoms i and j ³⁴ (it should be noted in ref 28, a non-Coulombic part is also included in this term to account for the exchange correlation and kinetic energy contributions), and r_{ij} is the separation of these two atoms. In a many-molecule system, the molecular energy is coupled with the intermolecular potential (usually only the Coulombic part) via the electronic configuration. The ground-state electronic configuration (Born–Oppenheimer limit) is located at the minimum of the sum of molecular and intermolecular energies.

Many nonpolarizable water force fields, such as SPC, SPC/E and TIP4P, were developed by fitting for liquid-state properties at ambient conditions, including internal energy, density, structure, and dielectric constant. Thus these effective force fields implicitly include a part describing the many-body effect of water at ambient conditions, and their transferability to other physical states (e.g. a low-density gas phase) or environments (e.g. inside a high-charge-density zeolite) is limited. In contrast, polarizable force fields are often developed by fitting to gas-phase properties (dipole moment, dimer energy) and liquid-phase properties. The reasoning behind this is that a force field that works at these two rather different thermodynamic states (with respect to density) should also yield a good description for intermediate densities. Recently, Kiyohara et al.³⁵ performed a series of Monte Carlo simulations in the grand canonical ensemble (using an iterative scheme to optimize the electronic configuration) to determine the near-critical phase envelopes for the Kozack and Jordan model,²⁰ the self-consistent point dipole polarizability (SCPDP) model of Chialvo and Cummings,²⁵ and point-polarizable SPC and TIP4P models. Medeiros and Costas³⁶ performed pseudo-Gibbs ensemble calculations for the TIP4P-FQ (fluctuating charge) force field in the temperature range 298 to 373 K. In addition, we performed adiabatic nuclear and electronic sampling Monte Carlo (ANES-MC) simulations in the Gibbs ensemble³⁷ to determine the vapor–liquid coexistence curves from 323 to 523 K for the SPC-FQ and TIP4P-FQ force fields.²⁴ Unfortunately, neither of these six polarizable models yielded satisfactory results for the vapor–liquid equilibria. Both simulation studies showed that neither the critical temperature nor the critical density is well reproduced by any of the polarizable force fields. Even more surprising, the fixed-charge SPC/E force field⁵ yielded much better predictions for the near-critical region of the phase diagram. In particular, we obtained critical constants of $T_c = 626 \pm 6$ K and $\rho_c = 0.312 \pm 0.012$ g/mL for the SPC/E model, relatively close to the experimental critical point of $T_c = 647$ K and $\rho_c = 0.322$ g/mL³⁸ and in good agreement with other simulation studies for this model.^{39,40} The disappointing performance of the dipole-polarizable and fluctuating-charge force fields demonstrates that fitting to properties of the liquid phase at ambient

conditions and to properties of gas-phase monomers and clusters is not sufficient to obtain force fields that are transferable to the entire fluid region of the phase diagram.

To improve the performance of some dipole-polarizable force fields, Kiyohara et al.³⁵ attempted to optimize the parameters for the Lennard–Jones (LJ) site on the oxygen atom. They found that very small changes in these parameters can result in dramatic changes in the location of the critical point, the saturated densities, and liquid structures, thereby emphasizing the importance of the short-range repulsive part of the LJ interactions. However, Kiyohara et al.³⁵ concluded that solely adjusting the LJ parameters was not sufficient to make any of the dipole-polarizable water models suitable for phase equilibrium calculations. Sparked by this, Errington and Panagiotopoulos⁴¹ developed a simple fixed-charge water model (which we call the EP model) using a Buckingham exp–6 potential for the van der Waals interactions that yields rather good phase equilibrium properties across a wide range of temperatures, but less satisfactory results for dielectric constants and liquid structures.

All polarizable water force fields (and, of course, also the fixed-charge water force fields) discussed previously use a fixed set of LJ parameters to describe the nonbonded van der Waals (vdW) interactions. However, a great deal of theoretical and experimental research^{42–45} has established a strong connection between vdW interactions of a molecule and its electronic configuration. Compared with the Coulombic interactions between partial charges, the contributions from the dispersive part of the vdW interactions is less important for aqueous systems. However, the repulsive part of the vdW interactions (arising from electron overlap) is significant for hydrogen-bonded systems in which the oxygen–oxygen distance is usually within the strongly repulsive region of the empirical force fields. The correlation between the vdW radius of a given atom and its charge state has been expressed using some empirical functional forms, and either exponential⁴⁵ or linear⁴² relationships are used most often. Recently, Badenhop and Weinhold⁴² calculated the repulsive sizes for a variety of atoms and ions in different molecules and found the linear dependence to yield better correlations than the exponential form. For example, slopes of -0.41 , -0.15 , and -0.16 Å/e were reported for hydrogen, fluorine, and chlorine, respectively.⁴² These nontrivial slopes demonstrate the large effect of variations of the electronic densities on the nonbonded vdW interactions. In contrast to the polarizable water models discussed so far, this effect is accounted for in molecular models based on the empirical valence bond approach and in shell models for ions. In the empirical valence bond approach, a molecule is generally represented by an effective two-state (a covalent state and an ionic state) description in which different nonbonded interactions parameters are used for these two states.^{46–49} In the shell models for ions, the separation between a nucleus and its (spherical) electron cloud is coupled by a harmonic spring and adjusts to the environment.⁵⁰

In this article, we show that coupling of the Lennard–Jones interaction parameters to the fluctuating partial charges on the oxygen atoms leads to significant improvements for the fluctuating-charge water models. The remainder of this article is arranged as follows. Sections 2 and 3 introduce the new polarizable models and give the simulation details, respectively. Results for vapor–liquid coexistence curves, second virial coefficients, energetics and average dipole moments of small clusters, liquid structures and densities close to ambient conditions, and dielectric constants are reported in Section 4. Finally, conclusions and an outlook to future water models are given.

2. SPC-pol and TIP4P-pol Water Force Fields

In this work, two different ways to couple the Lennard–Jones (LJ) interactions at oxygen atomic sites with the electronic configurations were investigated. Because the LJ potential can be expressed either in terms of σ and ϵ or A and C parameters (Of course, there is a simple mathematical relationship that converts from one form to the other.) as follows:

$$u_{\text{LJ}}(r_{ij}) = 4\epsilon_{ij} \left[\left(\frac{\sigma_{ij}}{r_{ij}} \right)^{12} - \left(\frac{\sigma_{ij}}{r_{ij}} \right)^6 \right] \quad (3a)$$

$$= \frac{A}{r_{ij}^{12}} - \frac{C}{r_{ij}^6} \quad (3b)$$

where r_{ij} is the separation of the two LJ sites i and j . Thus, we can make either σ and ϵ or A and C functions of the electronic configurations. On one hand, we follow the suggestion of Badenhoop and Weinhold⁴² and use a linear relationship between the vdW radius (here, σ_{ij}) and the charge magnitude (here, q_{iO} and q_{jO}), such that

$$\sigma_{ij} = a + b \times q_{\text{ave}} \quad (4a)$$

$$q_{\text{ave}} = \frac{q_{iO} + q_{jO}}{2} \quad (4b)$$

where a and b are the size of the neutral oxygen atom and the slope of the size/charge correlation, which are used as fitting parameters in this work. To keep the coupling simple, we assume that ϵ does not depend on the electronic configuration, i.e. ϵ remains fixed. However, the expansion of σ with respect to q introduces a nonquadratic charge-dependent term in the energy expression, which can cause sampling problems for the ANES-MC algorithm.^{37,51} Quadratic coupling of the electronic degrees of freedom to the nuclear degrees of freedom results in electronic phase volumes that are independent of nuclear configuration, thereby fostering the sampling of nuclear degrees of freedom from the Born–Oppenheimer limit.⁵¹ Therefore, we decided to approximate $(\sigma_{ij})^{12}$ and $(\sigma_{ij})^6$ by fitting to two separate quadratic spline functions as follows:

$$\sigma^{12} = \alpha_{12} + \beta_{12} \times q_{\text{ave}} + \gamma_{12} \times q_{\text{ave}}^2 \quad (5a)$$

$$\sigma^6 = \alpha_6 + \beta_6 \times q_{\text{ave}} + \gamma_6 \times q_{\text{ave}}^2 \quad (5b)$$

The specific values of the α , β , and γ constants will depend on the range of q_{iO} (or q_{ave}) used in the spline fit. Because we are interested in a water representation, we used 0.6, 0.8, and 1.0 e values (which are typical for the fluctuating-charge water force fields³⁷) for the spline fit, and did not consider the neutral oxygen atom.

The second route to couple LJ parameters to electronic structure is a direct expansion of the A and C parameters in eq 3.b with respect to q_{ave}

$$A = A_0 + A_1 \times q_{\text{ave}} + A_2 \times q_{\text{ave}}^2 \quad (6a)$$

$$C = C_0 + C_1 \times q_{\text{ave}} + C_2 \times q_{\text{ave}}^2 \quad (6b)$$

However, this would introduce six additional parameters, whereas only two parameters are required in eq 4a. Because fitting for these six parameters would be rather arduous, and because of the great importance of the repulsive part, we decided

to expand only the A parameter of eq 3b and, in addition, assumed that A_1 (in eq 6a) can be set to zero.

The SPC-FQ and TIP4P-FQ water models proposed by Berne and co-workers²⁴ were chosen as the prototypical fluctuating-charge water models. The details of these two models have been reported.^{24,37} Implementation of the two routes of coupling LJ parameters to oxygen partial charges is straightforward for the SPC-FQ and TIP4P-FQ models. For both coupling routes, only three new parameters [a , b , and ϵ (eqs 3a and 4a) or A_0 , A_2 , and C (eqs 3b and 6a)] remain for the fit to phase equilibrium properties. The fitting process was divided into parts. First, canonical ensemble ANES-MC simulations at $T = 298$ K and $\rho = 1.0$ g/mL were performed for a three-dimensional exploration for each of these two parameter sets. Liquid energies, densities, pressures, and average dipole moments were used to evaluate the parameters. Thereafter, the vapor–liquid coexistence curves for selected parameters sets were calculated from Gibbs ensemble ANES-MC simulations.

One benefit of coupling the LJ parameters to the fluctuating charges is obvious. Whereas for most polarizable force fields additional damping functions or hard-sphere potentials are required to avoid charge instabilities associated with close contacts of nonbonded partial charges, the coupling takes care of these unwanted effects because any dramatic increase of an oxygen charge is prevented by a concurrent growth of the repulsive vdW interactions.

3. Algorithms and Simulation Details

A. Algorithms. Simulations using polarizable models require that the system always remains in its electronic ground state, as prescribed by the Born–Oppenheimer (BO) approximation. Two rather different strategies can be used to achieve sampling from the BO limit (or to maintain an adiabatic separation of nuclear and electronic degrees of freedom) in simulations. First, iterative procedures^{23,27,35} or matrix inversion techniques^{36,51} can be used to minimize the electronic configuration for every change of nuclear configuration (molecular dynamics time step or single Monte Carlo move). Second, Car–Parrinello molecular dynamics approaches^{17,24,52–55} or the ANES-MC^{37,51} algorithm can be used; both treat the electronic configuration by fictitious classical degrees of freedom subject to a secondary low-temperature thermostat and involve an “on-the-fly” optimization of the electronic configuration during every nuclear move. Monte Carlo simulations using iterative procedures result in order N^3 scaling (where N is the number of the interaction sites in the system) of the computational requirements, thereby making simulations for polarizable models roughly N times more expensive than simulations for the parent fixed-charge force fields. Matrix inversion techniques are even more demanding, but offer the advantage of direct sampling of the nuclear configurations from the BO limit (whereas iterative methods only approach the BO limit). In contrast, the ANES-MC algorithm requires only a modest increase in computer time (by a factor 2 to 3), which is similar to the increase for molecular dynamics simulations of polarizable systems (considering that adequate sampling of the electronic degrees of freedom requires a reduction in time step).

B. Simulation Details. Canonical ensemble simulations for 100 water molecules at $T = 298$ K and $\rho = 1.0$ g/mL were performed to screen the LJ parameters (using approximately 10^5 MC cycles) and to calculate dielectric constants for the selected parameter sets (using more than 2×10^6 MC cycles for the production periods). Gibbs ensemble simulations^{56–58} for 120-molecule systems (using at least 10^5 MC cycles for the production periods) were performed at 373, 423, 473, 523, and

TABLE 1: Lennard–Jones Parameters for the SPC-pol and TIP4P-pol Force Fields^a

	A_1	A_3	C_1
SPC-pol-1	8	3	1200
SPC-pol-2	4	5	890
	a	b	ϵ
SPC-pol-3	2.665	0.5	135
TIP4P-pol-1	2.40	0.7	78
TIP4P-pol-2	2.60	0.5	95
TIP4P-pol-3	2.82	0.3	105

^a The units of A_1 , A_3 , C_1 , a , b , and ϵ are $5.92 \times 10^7 k_B K \text{ \AA}^{12}$, $5.92 \times 10^7 k_B K \text{ \AA}^{12}/e^2$, $5.92 \times 10^2 k_B K \text{ \AA}^6$, \AA , $\text{\AA}/e$, and $k_B K$. The internal geometries of these models are taken from the SPC and TIP4P force fields,^{4–6} and the fluctuating-charge parameters are taken without modification from the SPC-FQ and TIP4P-FQ force fields.²⁴

573 K to calculate the vapor–liquid coexistence curves. In addition, isobaric–isothermal ensemble simulations⁵⁹ for 100-molecule systems (using at least 3×10^6 MC cycles for the production periods) at $p = 1$ atm and $T = 223, 248, 273, 298, 323$, and 373 K were performed to search for the maximum in liquid density. For the LJ interactions, a spherical potential truncation for pair distances larger than 7.2 \AA was used for the canonical and Gibbs ensemble simulations, whereas a value of 7.0 \AA was used for the isobaric–isothermal ensemble simulations. Analytical tail corrections are added to approximate the remainder of the LJ interactions for all simulations. The Ewald parameters for all simulations were $\kappa \times L = 5$ and $K_{\max} = 5$.^{37,51} The maximum displacements for translational, rotational, and volume moves were adjusted to allow for efficient sampling from the BO skin using one electronic move at $T_{\text{elec}} = 5$ K or $T_{\text{elec}} = T_{\text{nucl}}$ per nuclear move.^{37,51} An additional preferential sampling strategy and 1000 electronic moves were used for the particle swap moves in Gibbs ensemble simulations using $T_{\text{elec}} = 5$ K.³⁷

4. Results and Discussion

A. Parameter Search. The primary goal of this work is to develop polarizable water force field for phase equilibrium calculations. The target properties are the saturated liquid and vapor densities, vapor pressures, and heats of vaporizations. The parameters being optimized are a , b , and ϵ , or A_1 , A_3 , and C_1 (see section 2). Compared with conventional polarizable force fields (fixed ϵ and σ for nonbonded interactions), only one additional parameter is introduced to allow for the coupling of the van der Waals interactions with the electronic configuration, but requires already a three-dimensional search in parameter space. Here we take advantage of the fact that any bad three-parameter combination simply can be ruled out by performing one single simulation at any thermodynamic state. Therefore canonical ensemble Monte Carlo simulations at $T = 298$ K and $\rho = 1.0$ g/mL were used to narrow the range of possible three-parameter combinations. In total, 174 parameter sets were tested, and the results are summarized in Tables S1 to S3 (Supporting Information). Six candidates (three based each on the SPC-FQ and TIP4P-FQ force fields²⁴) were selected from the search above based on the liquid energy, pressure, and average dipole moment, and their parameters are listed in Table 1.

B. Vapor–Liquid-Phase Equilibria. ANES-MC simulations^{37,51} in the Gibbs ensemble^{56–58} were performed to obtain the vapor–liquid coexistence curves from 373 to 573 K for the SPC-pol-1, SPC-pol-2, SPC-pol-3, TIP4P-pol-1, and TIP4P-pol-3 force fields. The corresponding phase diagrams are depicted in Figure 1 and the numerical data are listed in Table

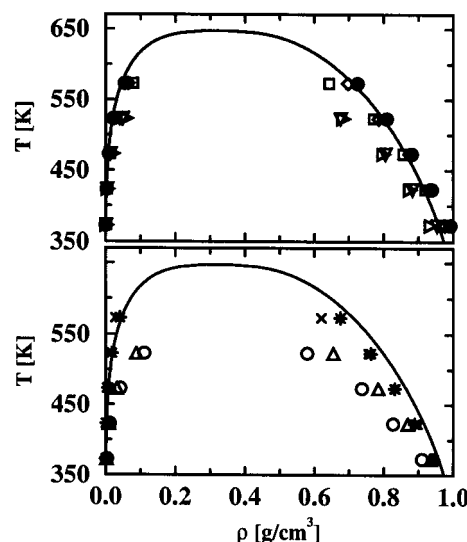


Figure 1. Saturated vapor and liquid densities. The solid line depicts the experimental coexistence densities.⁶⁰ Top: Simulation results for the SPC-pol-1 (filled circles), SPC-pol-2 (diamonds), SPC-pol-3 (squares), TIP4P-pol-1 (triangles down), and TIP4P-pol-3 (triangles right) force fields. Bottom: Simulation results for the SPC/E (×), SPC-FQ (circles), TIP4P-FQ (triangles up), and EP (stars) force fields.

TABLE 2: Numerical Results of the Gibbs Ensemble Simulations for Water Using the SPC-pol and TIP4P-pol Force Fields^a

T	$\langle P \rangle$	$\langle \rho_{\text{vap}} \rangle$	$\langle \rho_{\text{liq}} \rangle$	$\langle \mu_{\text{vap}} \rangle$	$\langle \mu_{\text{liq}} \rangle$	ΔH_{vap}
SPC-pol-1						
373	103 ₅	0.00060 ₃	0.992 ₁	1.89 ₃	2.45 ₁	41.0 ₃
423	593 ₄₅	0.0032 ₃	0.939 ₃	1.90 ₂	2.41 ₁	37.7 ₄
473	1900 ₆₀	0.0095 ₃	0.881 ₂	1.92 ₂	2.36 ₁	34.5 ₄
523	4430 ₂₄₀	0.022 ₂	0.809 ₃	1.94 ₁	2.32 ₁	30.2 ₆
573	10200 ₄₀₀	0.055 ₄	0.725 ₅	1.97 ₂	2.27 ₁	24.6 ₁₀
SPC-pol-2						
373	155 ₁₃	0.00091 ₈	0.977 ₉	1.87 ₁	2.39 ₁	40.4 ₁
423	750 ₇₀	0.0041 ₃	0.930 ₁₀	1.88 ₁	2.34 ₁	36.8 ₄
473	2460 ₂₃₀	0.013 ₂	0.874 ₅	1.88 ₁	2.30 ₁	33.1 ₇
523	5200 ₅₈₀	0.026 ₃	0.786 ₁₃	1.91 ₂	2.25 ₁	29.2 ₅
573	11200 ₆₀₀	0.065 ₅	0.698 ₁₈	1.97 ₂	2.19 ₂	23.1 ₁₀
SPC-pol-3						
373	155 ₆	0.00093 ₄	0.975 ₂	1.90 ₁	2.44 ₁	40.1 ₂
423	638 ₂₇	0.0035 ₂	0.920 ₁	1.91 ₂	2.40 ₁	36.8 ₃
473	2270 ₉₀	0.012 ₁	0.857 ₃	1.94 ₂	2.37 ₁	32.7 ₆
523	5780 ₁₆₀	0.032 ₂	0.772 ₅	1.95 ₁	2.32 ₁	28.3 ₅
573	12200 ₃₀₀	0.079 ₅	0.644 ₁₀	2.02 ₂	2.28 ₂	21.7 ₆
TIP4P-pol-1						
373	173 ₁₃	0.0010 ₁	0.954 ₃	1.92 ₃	2.31 ₁	39.4 ₃
423	734 ₃₇	0.0042 ₂	0.883 ₁₀	1.92 ₂	2.29 ₁	35.3 ₅
473	2430 ₇₀	0.014 ₁	0.805 ₄	1.93 ₃	2.26 ₁	30.2 ₅
523	6740 ₃₇₀	0.049 ₆	0.676 ₈	2.00 ₅	2.22 ₁	20.6 ₈
TIP4P-pol-3						
373	275 ₁₃	0.0017 ₁	0.935 ₄	1.90 ₁	2.40 ₁	38.4 ₄
423	1122 ₄₈	0.0063 ₃	0.876 ₄	1.92 ₁	2.36 ₁	34.4 ₄
473	3640 ₁₀₀	0.021 ₁	0.799 ₄	1.94 ₁	2.32 ₁	29.2 ₄
523	8750 ₂₆₀	0.059 ₃	0.684 ₆	2.00 ₂	2.27 ₁	21.6 ₈

^a Temperatures, (vapor) pressures, orthobaric densities, dipole moments, and heats of vaporization are given in units of K, kPa, g/mL, Debye, and kJ/mol, respectively. The subscripts give the statistical accuracies of the last decimal(s).

2. The SPC-pol-1 and SPC-pol-2 force fields yield the best results for saturated liquid densities, in particular, at the higher temperatures, whereas the SPC-pol-3 and TIP4P-pol force fields show large deviations in the saturated liquid densities at the higher temperatures. However, from Figure 1 it is apparent that the SPC-pol force fields yield too high liquid densities below

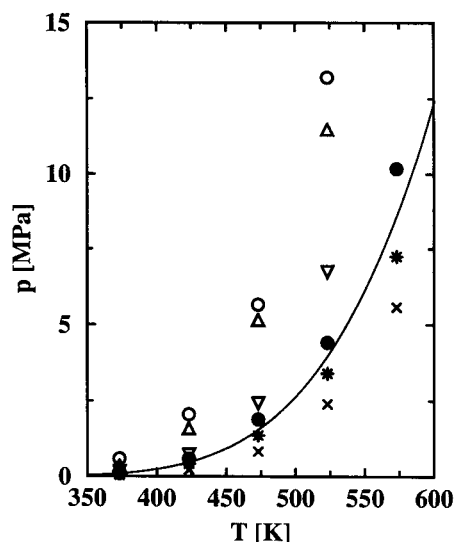


Figure 2. Comparison of the vapor pressures calculated for the SPC/E (\times), SPC-FQ (circles), SPC-pol-1 (filled circles), TIP4P-FQ (triangles up), TIP4P-pol-1 (triangles down), and EP (stars) force fields. The solid line represents the experimental data.⁶⁰

the boiling point. Estimates of the critical temperatures⁵⁸ also demonstrate satisfactory agreement with experiment for the SPC-pol-1 (650 K), SPC-pol-2 (630 K), and SPC-pol-3 (620 K) force fields, whereas the predictions for the TIP4P-pol-1 (580 K) and TIP4P-pol-3 (580 K) force fields are significantly too low, but still higher than for the original SPC-FQ (540 K) and TIP4P-FQ (560 K) force fields.³⁷ These estimates of the critical temperatures have an uncertainty of approximately 2%, which arises from the statistical errors of the simulation results and from the extrapolation procedure.

The saturated vapor pressures calculated for the SPC-pol and TIP4P-pol force fields are compared with experiment and other force fields in Figure 2. Although the fixed-charge SPC/E force field yields consistently too low vapor pressures (by about a factor of 2), the SPC-FQ force field suffers from far too high vapor pressures (typically a factor of 3 too high). In contrast, the fixed-charge EP force field leads to excellent predictions of the vapor pressures. Only the SPC-pol-1 force field comes close to the performance of the EP model, whereas the SPC-pol-2, SPC-pol-3, and TIP4P-pol force fields give noticeably too high vapor pressures. Using fits to the Clausius–Clapeyron equation, the following boiling points were estimated: SPC/E (397 ± 1 K), SPC-FQ (333 ± 2 K), TIP4P-FQ (338 ± 2 K), SPC-pol-1 (370 ± 3 K), SPC-pol-2 (358 ± 2 K), SPC-pol-3 (361 ± 3 K), TIP4P-pol-1 (359 ± 2 K), and TIP4P-pol-3 (345 ± 2 K). Again, the performance of the SPC-pol-1 force field is excellent, yielding a boiling point that is only a few degrees Kelvin too low. The other two SPC-pol and the TIP4P-pol-1 force fields underestimate the normal boiling point by less than 5%, whereas the original SPC-FQ and TIP4P-FQ models yield vapor pressures and boiling points that make them unsuitable for phase equilibrium calculations.

The trends discussed for the saturated liquid densities and vapor pressures are mirrored by the heats of vaporization (see Figure 3). The SPC/E model substantially overestimates the heats of vaporization at the lower temperatures, but approaches the experimental values at the higher temperatures. This is not surprising, because the energy cost to polarize the water molecules (from monomer to bulk liquid) was implicitly included in the fit of the SPC/E force field.⁵ However, because the difference in polarization costs is not considered for the vapor phase, the heats of vaporization come out too high. In

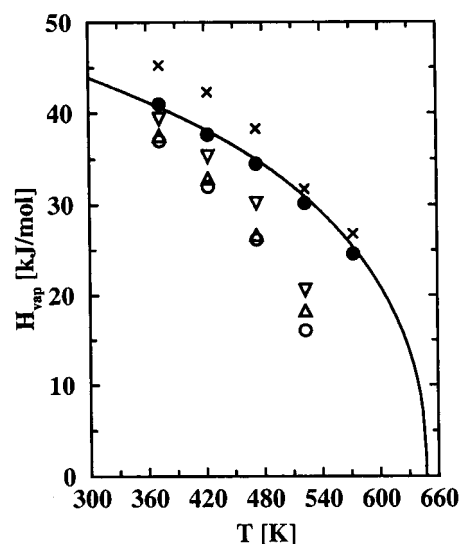


Figure 3. Comparison of the heats of vaporization calculated for the SPC/E (\times), SPC-FQ (circles), SPC-pol-1 (filled circles), TIP4P-FQ (triangles up), and TIP4P-pol-1 (triangles down) force fields. The solid line represents the experimental data.⁶⁰

contrast to the SPC/E force field, the SPC-FQ force field gives good agreement with experiment at the lower temperature (in particular, at ambient conditions), but the heat of vaporization changes too rapidly with temperature and is, for example, 10 kJ/mol too low at 523 K. In particular, the SPC-pol-1 force field excels in this respect, and consistently predicts satisfactory results across the entire temperature range. The heats of vaporization obtained for the SPC-pol-2 and SPC-pol-3 force fields are acceptable, albeit not as good as for the SPC-pol-1 force field, whereas the TIP4P-pol-1 force field shows too rapid changes with temperature (as should be expected from its too low critical temperature).

In summary, the results for vapor–liquid-phase equilibria (saturated liquid densities, vapor pressures, and heats of vaporization) show that the additional coupling of Lennard–Jones parameters to the fluctuating charges leads to significant improvements over the SPC-FQ and TIP4P-FQ force fields. With the exception of the SPC-pol-1 force field, none of the polarizable force fields gives results that match up with the excellent performance of the fixed-charge EP force field that was optimized for phase equilibrium calculations.⁴¹

C. Second Virial Coefficients and Minimum-Energy Clusters. Whereas the vapor–liquid phase diagram is governed by the energetic difference between bulk vapor and liquid phases, the second virial coefficient probes only the interactions of dimers. However, the second virial coefficient is a much better test of dimer interactions than calculations of the dimer binding energy (see below), because the former probes the interactions Boltzmann-averaged over separations and orientations, whereas the latter is only based on a single dimer configuration. Obviously, the strengths of the many-body polarization effect are very different for bulk liquid water and a dimer, and thus one should not expect fixed-charge force fields to do well in this respect. Indeed, the SPC/E model yields second virial coefficients that are substantially too large in magnitude (see Figure 4), because it is built around partial charges that are not representative for the water dimer. However, the performance of the fixed-charge EP force field is significantly better than those of the SPC/E and other fixed-charge force fields.⁴¹ In contrast, both the SPC-FQ and TIP4P-FQ force fields give second virial coefficients that are significantly too small in magnitude (see Figure 4). It has already been noted that these

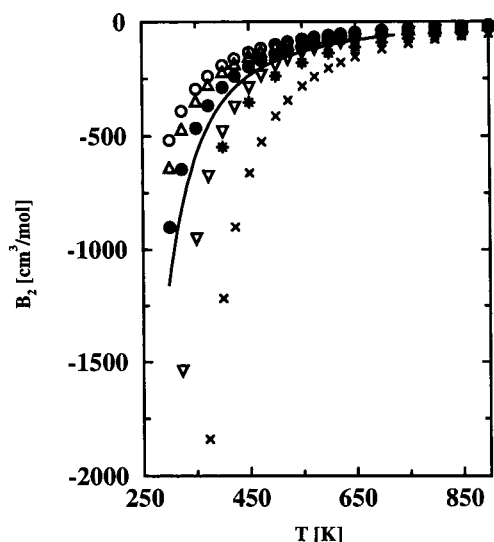


Figure 4. Comparison of the second virial coefficients calculated for the SPC/E (\times), SPC-FQ (circles), SPC-pol-1 (filled circles), TIP4P-FQ (triangles up), TIP4P-pol-1 (triangles down), and EP (stars) force fields. The solid line represents the experimental data.⁷¹

two polarizable force fields²⁴ underestimate the binding energy of the water dimer by about 20%. In contrast, the SPC-pol-1 force field gives much better agreement with the experimental second virial coefficient across a wide range of temperatures (300–900 K). The TIP-pol-1 force field performs adequately at the higher temperatures, but yields values that are too large below 400 K. Here we would like to argue that electronic polarizability and coupling of the vdW interactions are required to yield good agreement with experiment. For example, the SPC/E force field performs poorly because the magnitudes of the partial charges are too large for a water dimer, and the vdW interactions of the SPC-FQ model are too repulsive for the water dimer because there is no coupling between Lennard–Jones parameters and fluctuating charges.

Similar conclusions are also supported by comparison of the properties of small, minimum-energy water clusters (see Table 3). The dimer binding energy obtained for the SPC/E force field is more than 30% too large, whereas it is too small for the SPC-FQ force field. With the exception of the TIP4P-pol-1 force field, the SPC-pol and TIP4P-pol force fields give binding energies that agree to within (experimental) uncertainty with the experimental value of -22.6 ± 2.9 kJ/mol.⁶¹ All polarizable water force fields show a large enhancement of the average molecular dipole moment in the dimer compared with the monomer. The SPC-FQ and the three SPC-pol models yield values between 2.09 and 2.11 D in excellent agreement with a value of 2.10 D predicted from ab initio calculations.¹ Whereas the molecular dipole moments obtained for the TIP4P-pol models are slightly too low (2.05–2.07 D), these models favor a water dimer structure that is substantially more bent (as measured by the acceptor angle) and is in much better agreement with the experimentally determined water dimer structure. The apparent lack of such a tetrahedral association for the SPC-pol models negatively impacts their ability to describe the liquid water structure near ambient conditions (see section 4.D).

A great deal of both experimental and theoretical research is targeted on small water clusters.^{1–3,61,62} It is now well-known that small clusters exhibit many of the molecular details associated with the complex behavior of the liquid phase, such as the cooperativity in hydrogen bonding, hydrogen-bond network arrangements, and aqueous solvation.³ From ab initio calculations it was concluded that the average molecular dipole

moment increases from 1.85 D for the monomer to 2.70 D for the cyclic hexamer.¹ This huge enhancement demonstrates the importance of including polarization effects in empirical water models. We obtained cluster binding energies, average molecular dipole moments, and average oxygen–oxygen separations for the SPC/E, SPC-FQ, SPC-pol, and TIP4P-pol force fields via simulated annealing for clusters containing two to six water molecules (see Table 3). The cluster-size-dependent change in molecular dipole moments is best described by the SPC-pol-1 model, which gives quantitative agreement with the ab initio calculations.¹ In contrast, the SPC-FQ model overestimates the increase in dipole moments (with a value of 2.91 D for the cyclic hexamer), whereas the TIP4P-pol-1 model greatly underestimates the polarization effect (with a value of 2.42 D for the cyclic hexamer). In particular, for the three TIP4P-pol force fields the effect of changing the slope of the LJ-diameter/fluctuating-charge coupling is evident. The TIP4P-pol-1 model with $b = 0.7$ Å/e is far less polarizable than the TIP4P-pol-3 model with $b = 0.3$ Å/e. On the energetic side, all polarizable force fields predict little cooperativity for the relatively strained trimer; that is, the binding energy resulting from the formation of three hydrogen bonds, to a good approximation, is equal to three times the dimer binding energy. However, the larger clusters show a pronounced cooperative effect with the tetramer binding energy being approximately five times that for the dimer (between 4.9 for TIP4P-pol-1 and 5.5 for SPC-FQ), and the corresponding factors for the pentamer range from 6.7 (for TIP4P-pol-1) to 8.0 (for SPC-FQ), and for the hexamer from 9.4 (for TIP4P-pol-1) to 10.0 (for SPC-FQ). Again, decreases in the b parameters yield systematic increases in the magnitude of the cooperative effect for the three TIP4P-pol force fields. As should be expected, the SPC/E force field yields much smaller enhancements with ratios of 4.5, 6.0, and 7.4 for tetra-, penta-, and hexamer, respectively. The corresponding values obtained from high-level ab initio calculations are 5.7, 7.5, and 9.4 for tetra-, penta-, and hexamer.² In particular, the SPC-pol-1 and TIP4P-pol-3 force fields agree very well with the ab initio calculations, not only with respect to the cooperativity ratios discussed above, but also with respect to the absolute binding energies themselves (giving mean percentage deviations of less than 5%).

Although average oxygen–oxygen separations decrease by 0.22 Å from dimer to hexamer for the SPC-FQ force field, the corresponding decreases for the SPC-pol and TIP4P-pol force fields are only about 0.1 Å, and the SPC/E model gives a shortening by only 0.03 Å. The experimentally measured decrease in oxygen–oxygen separation is 0.23 Å,^{1,3} in good agreement with the ab initio calculations.^{1,2} However, much of this decrease is found for the step from dimer to trimer. In contrast, the oxygen–oxygen separations for dimer and trimer are very close (within 0.02 Å) for all polarizable models studied here, but a dramatic decrease is found when a tetramer is formed. Besides these relative trends, significant differences in the oxygen–oxygen distances can be observed between experimental results and high-level ab initio calculation, with the latter yielding values that are on average about 0.06 Å shorter. The SPC-pol-1 force field predicts oxygen–oxygen separations for the tri-, tetra-, and pentamer that, maybe fortuitously, agree with experiment to within 0.01 Å, but its dimer bond length is substantially too short by 0.1 Å. The SPC-FQ force field performs as well as the SPC-pol-1 force field, but the other SPC-pol and TIP4P-pol models do much worse.

Despite the good agreement with experimental data and ab initio calculations for the cooperative effects discussed above,

TABLE 3: Properties of Minimum-Energy Water Clusters and Bulk Liquid Water Obtained for Different Force Fields^a

	SPC-pol-1	SPC-pol-2	SPC-pol-3	TIP4P-pol-1	TIP4P-pol-2	TIP4P-pol-3	SPC/E	SPC-FQ	Exp	AI
Monomer										
μ	1.85	1.85	1.85	1.85	1.85	1.85	2.35	1.85	1.85	1.85
Dimer										
\bar{E}	-20.9	-22.3	-24.3	-26.0	-24.1	-22.2	-30.1	-18.4	-22.6	-21.2
$\bar{\mu}$	2.09	2.11	2.11	2.05	2.06	2.07	2.35	2.09		2.10
r_{OO}	2.88	2.78	2.73	2.69	2.71	2.77	2.73	2.94	2.98	2.93
θ_{don}	52.5	52.9	53.1	54.9	54.9	54.9	52.9	52.2	51	
θ_{acc}	14.1	13.7	13.4	40.3	40.3	40.2	18.5	14.3	57	
Trimer										
\bar{E}	-59.6	-65.2	-68.6	-69.9	-65.3	-61.2	-82.0	-53.1		-65.9
$\bar{\mu}$	2.28	2.28	2.28	2.16	2.18	2.21	2.35	2.31		2.30
r_{OO}	2.88	2.80	2.75	2.70	2.71	2.77	2.74	2.92	2.87	2.78
Tetramer										
\bar{E}	-112	-122	-128	-127	-120	-114	-136	-103		-120
$\bar{\mu}$	2.52	2.51	2.49	2.31	2.34	2.39	2.35	2.62		2.55
r_{OO}	2.79	2.72	2.69	2.63	2.68	2.72	2.70	2.79	2.80	2.74
Pentamer										
\bar{E}	-156	-171	-174	-174	-164	-157	-178	-147		-160
$\bar{\mu}$	2.65	2.64	2.57	2.38	2.42	2.48	2.35	2.80		2.66
r_{OO}	2.76	2.69	2.68	2.62	2.67	2.70	2.70	2.74	2.75	2.71
Hexamer										
\bar{E}	-193	-212	-216	-217	-205	-196	-222	-184		-199
$\bar{\mu}$	2.70	2.69	2.62	2.42	2.46	2.53	2.35	2.91		2.70
r_{OO}	2.75	2.68	2.67	2.61	2.66	2.69	2.71	2.72		2.70
Liquid State ($T = 298 \text{ K}$, $\rho = 1.0 \text{ g/mL}$)										
$\langle E \rangle$	-41.6	-41.6	-41.7	-42.0	-41.3	-41.1	-46.8	-41.4	-41.4	
$\langle m \rangle$	2.51	2.43	2.48	2.31	2.36	2.45	2.35	2.83		

^a The minimum energy, (average) molecular dipole moment, (average) oxygen–oxygen separation, and characteristic dimer donor and acceptor angles (θ_{don} and θ_{acc} as defined in refs 26 and 61) are given in units of kJ/mol, Debye, Å, and degrees, respectively. Experimental data and results of ab initio calculations are taken from refs 1, 2, 3, and 61.

the minimum-energy configurations predicted by the SPC-pol force fields are quite different from those predicted from ab initio calculations¹ and inferred from spectroscopic data.³ In particular, for the trimer, tetramer, and pentamer, the structures obtained for the SPC-pol force fields are too flat with most hydrogen atoms lying close to the oxygen plane. The TIP4P-pol force fields, on the contrary, predicted minimum-energy configurations which resemble closely those obtained from ab initio calculation.¹

D. Radial Distribution Functions and Liquid Densities.

The oxygen–oxygen, oxygen–hydrogen, and hydrogen–hydrogen radial distribution functions (RDFs) clearly demonstrate the uniqueness of liquid water marked by the tetrahedral arrangement of strong hydrogen bonds. Thus reproducing experimentally obtained RDFs has always been one of the most important tests for any empirical water force field.⁶³ Canonical ensemble simulations at ambient conditions ($T = 298 \text{ K}$ and $\rho = 1.0 \text{ g/cm}^3$) were used to calculate the RDFs for the SPC/E, SPC-FQ, SPC-pol-1, and TIP4P-pol-1 force fields (see Figures 5 to 7). All these models yield a qualitatively correct description of the first hydrogen-bonded shell, but the peak height of the first peak in the O–O RDF is overestimated by all models, and the peak position differs slightly (experiment, 2.84 Å^{64,65}; SPC/E, 2.74 Å; SPC-FQ, 2.79 Å; SPC-pol-1, 2.87 Å; TIP4P-pol-1, 2.72 Å). However, for the SPC-FQ and SPC-pol-1 the O–O peaks for the second and third solvation shells are absent, but they are reproduced quite well by the SPC/E and TIP4P-pol-1 models. Here we speculate that the loss of long-range structure observed for the SPC-FQ and SPC-pol force fields is probably due to the large increase of the LJ ϵ parameter compared with the SPC/E model, which gives more importance to the LJ interactions and results in a more spherical shape of the SPC-FQ and SPC-pol-1 water molecules. In agreement with many

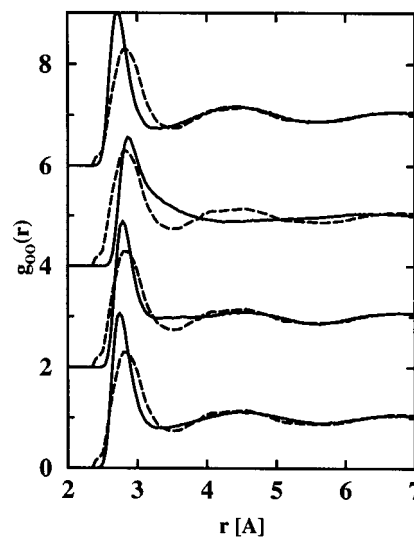


Figure 5. Oxygen–oxygen radial distribution functions (at $T = 298 \text{ K}$ and $\rho = 1.0 \text{ g/mL}$) calculated for the SPC/E, SPC-FQ (vertically offset by 2 units), SPC-pol-1 (vertically offset by 4 units), and TIP4P-pol-1 (vertically offset by 6 units) force fields. For comparison, results of neutron diffraction experiments⁶⁴ are shown as dashed lines.

other simulation studies, the TIP4P, TIP4P-FQ, and TIP4P-pol force fields show a more tetrahedral arrangements (see also Table 3), which is attributed to the displacement of the oxygen partial charge along the bisector toward the hydrogen atoms.

As already noticed for the O–O RDF, the empirical force fields tested in this study all appear to overestimate the structure of the first hydrogen-bonded shell. This is also evident from the O–H and H–H RDFs, where the first peaks generally are too high and the first valleys too low. However, small, but

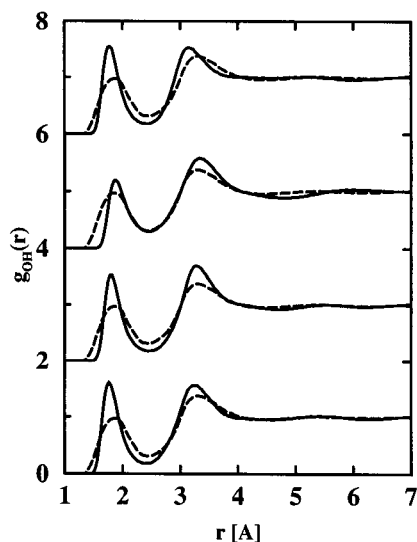


Figure 6. Oxygen–hydrogen radial distribution functions at $T = 298$ K and $\rho = 1.0$ g/mL. Simulation and experimental results shown with the same line styles and offsets as in Figure 5.

noticeable differences exist between the force fields. In particular, it appears that the SPC-pol-1 force field gives a slightly better representation of the O–H and H–H structures with the following characteristics (corresponding experimental data in brackets): position and height of first peak in O–H RDF, 1.88 Å and 1.19 (1.85 Å and 0.97); height of first valley in O–H RDF, 0.28 (0.31); position and height of first peak in H–H RDF, 2.51 Å and 1.29 (2.39 Å and 1.18); and height of first valley in H–H RDF, 0.88 (0.80).

Isobaric–isothermal ensemble Monte Carlo calculations at standard pressure and for temperatures ranging from 223 to 373 K were performed for the SPC-pol-1, SPC-pol-2 and the three TIP4P-pol force fields (see Table 4 and Figure 8). As has been also observed in recent simulation studies^{66–69} for the SPC, SPC/E, TIP3P, and TIP4P force fields, the minimalistic three-site force fields do not produce a density maximum close to the experimental freezing point. Whereas the SPC-pol-1 and SPC-pol-2 force fields give the best results for the saturated liquid densities from 373 to 573 K (see section 4.B), they yield rather poor results for the liquid densities near ambient temperatures. In contrast to the SPC-type force fields, the original TIP4P model and all three TIP4P-pol force fields clearly show a maximum in the liquid density. In particular, the three TIP4P-pol force fields predict a density maximum for temperatures close to 277 K, and the asymmetry in the density–temperature curve compares favorably with experiment.⁷⁰ However, the decrease in density from 273 to 373 K is significantly too large for all TIP4P-based models.

For further analysis of the cause for the density maximum, the oxygen–oxygen RDFs for the TIP4P-pol-1 model are shown as a function of temperature in Figure 9. The lower the temperature, the stronger and more uniform is the tetrahedral arrangement of the water molecules with more pronounced long-range ordering (appearance of peaks for the second and third solvation shell). The corresponding number integrals of the oxygen–oxygen RDFs at $T = 223$ and 298 K are shown in Figure 10. Because of the more regular tetrahedral arrangement of the water molecules, there is a distinct, solidlike plateau between the first and second shells at $T = 223$ K. The extended tetrahedral network excludes some space and leads to a lowering of the number of neighboring water molecules beyond the second solvation shell, which in turn produces the unusual phenomenon of a decrease in liquid density with increasing temperature.

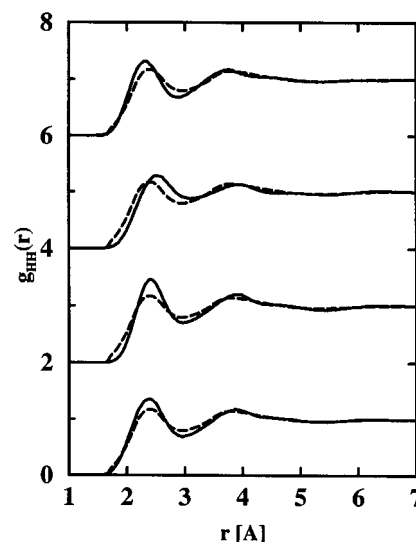


Figure 7. Hydrogen–hydrogen radial distribution functions at $T = 298$ K and $\rho = 1.0$ g/mL. Simulation and experimental results shown with the same line styles and offsets as in Figure 5.

E. Dielectric Constants. Dielectric constants were evaluated for the SPC/E, SPC-FQ, SPC-pol, and TIP4P-pol force fields at $T = 298$ K and $\rho = 1.0$ g/cm³. Whereas the dielectric constant for the fixed-charge SPC/E model is 15% too low (67 ± 2 , in good agreement with other simulation studies^{10,41}), the corresponding value for the polarizable SPC-FQ model is far too high (114 ± 6 , in good agreement with the result of molecular dynamics simulations²⁴). The dielectric constants at ambient conditions calculated for the SPC-pol force fields fall between those for the SPC/E and SPC-FQ force fields, but are 15–25% too high. In contrast, the dielectric constant for the TIP4P-pol-3 model is estimated to be 10% too low. As noted previously,^{10,11} a strong correlation seems to exist between the magnitude of the average molecular dipole moment of a given molecular model and its resulting dielectric constant. However, as seen from comparison of the SPC-pol-2 and TIP4P-pol-3 force fields that have average molecular dipole moments that agree to within 1%, but dielectric constants that differ by almost 30%, other factors (such as the intramolecular structure) also must play an important role.

As mentioned in the Introduction, the precise value of the average molecular dipole moment for liquid water at ambient conditions has not yet been determined experimentally and has been the subject of intense controversy. Recently, a value of 3.0 D (with a relatively broad distribution) was obtained from first-principle molecular dynamics simulations of 64 water molecules (at $T = 318$ K).^{15,16} Our simulation studies agree with respect to the broad charge distribution (not shown, but see ref 37), but disagree on the magnitude of the dipole moment. From our results we would like to infer that average molecular dipole moments of about 2.4 and 2.5 D would be desirable for a SPC-pol or a TIP4P-pol force field, respectively, to yield the correct dielectric constant. One potential source for the disagreement between empirical models and the first-principle representation could have its origin in the use of simple partial charges to represent the complex electronic structure of a molecule. However, for the minimum-energy water clusters (see section 4.C), there is very good agreement between the molecular dipole moments obtained from ab initio calculations^{1,2} and those obtained for the empirical SPC-pol-1 force field. Thus, at least for the polarizable models studied here, we observe that the average molecular dipole moment in liquid water at ambient conditions is smaller than that of the minimum-energy hexamer.

TABLE 4: Liquid Water Densities (in Units of g/mL) Obtained from Isothermal–Isobaric Simulations at $p = 1 \text{ atm}^a$

T (K)	SPC-pol-1	SPC-pol-2	TIP4P-pol-1	TIP4P-pol-2	TIP4P-pol-3	Exp
223			0.994 ₄	0.984 ₅	0.991 ₇	
248	1.093 ₆	1.073 ₄	1.013 ₃	1.011 ₅	1.003 ₅	0.9896
273	1.080 ₂	1.066 ₅	1.015 ₄	1.014 ₃	1.003 ₃	0.9998
298	1.066 ₂	1.057 ₃	1.011 ₂	1.003 ₂	0.995 ₂	0.9970
323		1.043 ₂	1.001 ₂	0.987 ₃	0.982 ₂	0.9880
348			0.981 ₂		0.962 ₂	0.9748
373			0.958 ₂	0.952 ₂	0.939 ₂	0.9584

^a Experimental results are taken from ref 70. The subscripts give the statistical accuracy of the last decimal.

TABLE 5: Dielectric Constants of Liquid Water Obtained from Canonical Ensemble Simulations at the Experimental Saturated Liquid Densities^a

T (K)	ρ (g/mL)	SPC/E	SPC-FQ	SPC-pol-1	SPC-pol-2	SPC-pol-3	TIP4P-pol-1	TIP4P-pol-3	Exp
298	1.0	67 ₂	114 ₆	98 ₆	89 ₂	88 ₅	50 ₅	69 ₁₂	77.7
473	0.865			35.1 ₆	34.7 ₈	34.3 ₁₀			34.8
570	0.718			20.0 ₄	19.6 ₅	21.0 ₃			20.7

^a Experimental data are taken from ref 72. The subscripts give the statistical accuracy of the last decimal(s).

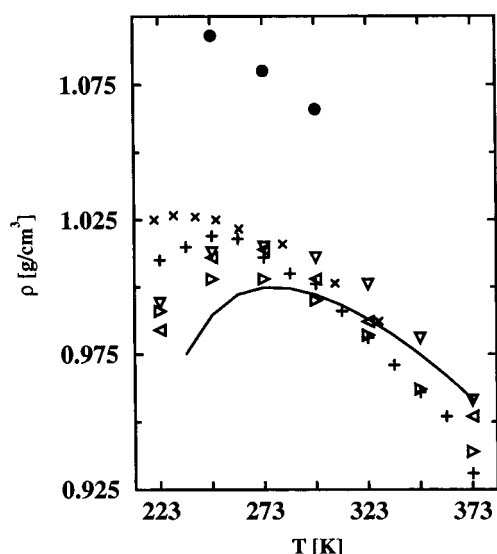


Figure 8. Specific density versus temperature plots for liquid water at $p = 1 \text{ atm}$ calculated for the SPC/E (\times),⁶⁶ TIP4P (pluses),⁶⁸ SPC-pol-1 (filled circles), TIP4P-pol-1 (triangles down), TIP4P-pol-2 (triangles left), and TIP4P-pol-3 (triangles right) force fields. The experimental data⁷⁰ are depicted by a solid line.

This might be plausible considering that the average nearest neighbor oxygen–oxygen separation is larger in liquid water³ than in the minimum-energy hexamer.¹

For the SPC-pol models, the dielectric constants were also calculated at $T = 473 \text{ K}$ and at 570 K using canonical ensemble simulations at the experimental saturated liquid densities. The experimental saturated liquid densities across this temperature range are well reproduced by the SPC-pol-1 and SPC-pol-2 force fields, but the SPC-pol-3 force field yields liquid densities that are significantly smaller. The high-temperature dielectric constants for the three SPC-pol force fields are within a few percent of each other and, maybe fortuitously, agree extremely well with the experimental results. Thus, when the entire coexistence region from ambient to near-critical temperatures is considered, the SPC-pol force fields appear to give better agreement for the dielectric constant than the SPC-FQ, TIP4P-FQ, or EP force fields.

5. Conclusions

A simple modification to the SPC-FQ and TIP4P-FQ water force field developed by Rick et al.²⁴ is suggested which allows

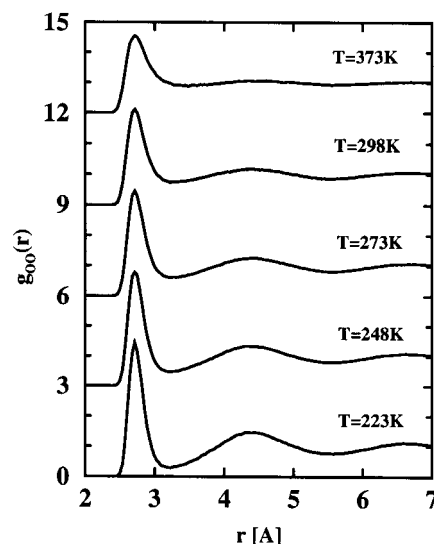


Figure 9. Temperature evolution of the oxygen–oxygen radial distribution functions calculated for the TIP4P-pol-1 force field at $p = 1 \text{ atm}$.

for the coupling of the Lennard–Jones parameters to the magnitude of the partial charges on oxygen atoms. This coupling has its quantum-mechanical origin in the charge-magnitude dependence of the overlap integrals. The additional size/charge coupling leads to significant improvements in the performance of polarizable water models throughout the entire fluid region of the phase diagram. In particular, the SPC-pol-1 force field proposed here gives satisfactory predictions for the saturated vapor and liquid densities, vapor pressures, heats of vaporization, second virial coefficients, and binding energies and dipole moments for small minimum-energy clusters. However, this and the other SPC-pol force fields yield low-temperature liquid densities that are substantially too high and do not produce a density maximum. Furthermore, their structures for the minimum-energy clusters are too flat, and their liquid structures do not show tetrahedral structure beyond the first solvation shell. In contrast, the TIP4P-pol force fields give a better representation of the minimum-energy cluster structures and of the liquid structures at near-ambient temperatures. However, their saturated liquid densities and heats of vaporization decrease too rapidly with increasing temperature, which leads to an unsatisfactory representation of the phase diagram in the near-critical region. In summary, although we can recommend the SPC-pol-1 force field for phase equilibrium calculations at elevated temperatures

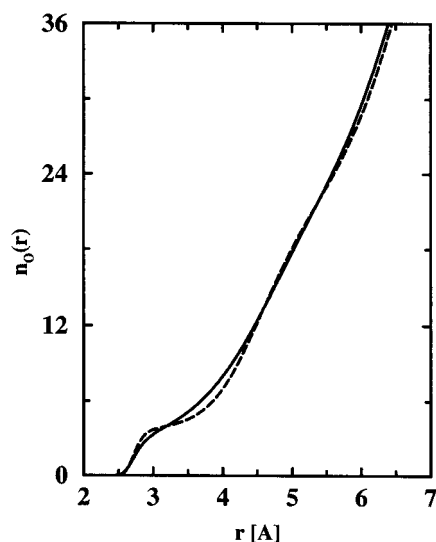


Figure 10. Number integrals of the oxygen–oxygen radial distribution functions calculated for the TIP4P-pol-I force field at $p = 1$ atm and $T = 223$ K (dashed line) and 298 K (solid line).

(above 400 K), this investigation did not result in a simple, polarizable force field that works satisfactorily from the triple point to the boiling point of water.

Thus we have to continue our quest for improved water force fields. The somewhat disappointing results obtained for the models based on the three-site SPC and four-site TIP4P representations, lead us to conclude that neither three nor four sites are sufficient. A better representation of the water molecule could involve the use of additional (polarizable) charge sites on the oxygen lone pairs, of an anisotropic or multisite representation of the van der Waals interactions, and of an additional coupling of the intramolecular structure to the electronic environment.

Acknowledgment. We thank Michele Parrinello, Woods Halley, Darrin York, and Wilfred van Gunsteren for many stimulating discussions. Financial support from the National Science Foundation (CTS-9813601), a Camille and Henry Dreyfus New Faculty Award, a McKnight/Land-Grant Fellowship, an Alfred P. Sloan Research Fellowship, a Stanwood Johnston Memorial Fellowship (B.C.), and a Dissertation Fellowship (B.C.) is gratefully acknowledged. Part of the computer resources were provided by the Minnesota Supercomputing Institute.

Supporting Information Available: Tables of the short canonical-ensemble simulations. This information is available free of charge via the Internet at <http://pubs.acs.org>.

References and Notes

- Gregory, J. K.; Clary, D. C.; Liu, K.; Brown, M. G.; Saykally, R. *J. Science* **1997**, 275, 814.
- Gregory, J. K.; Clary, D. C. *J. Phys. Chem.* **1996**, 100, 18014.
- Liu, K.; Cruzan, D.; Saykally, R. *J. Science* **1996**, 271, 929.
- Berendsen, H. J. C.; Postma, J. P. M.; van Gunsteren, W. F.; Hermans, J. In *Intermolecular Forces*; Pullman, B., Ed.; Reidel: Dordrecht, 1981; p 331.
- Berendsen, H. J. C.; Grigera, J. R.; Straatsma, T. P. *J. Phys. Chem.* **1987**, 91, 6269.
- Jorgensen, W. L.; Chandrasekhar, J.; Madura, J. D.; Impey, R. W.; Klein, M. L. *J. Chem. Phys.* **1983**, 79, 926.
- Clough, S. A.; Beers, Y.; Klein, G. P.; Rothman, L. S. *J. Chem. Phys.* **1973**, 59, 2254.
- Xantheas, S. S.; Dunning, T. H., Jr. *J. Chem. Phys.* **1993**, 99, 8874.
- Carnie, S. L.; Patey, G. N. *Mol. Phys.* **1982**, 47, 1129.
- Watanabe, K.; Klein, M. L. *Chem. Phys.* **1989**, 131, 157.
- Sprick, M. *J. Phys. Chem.* **1991**, 95, 2283.
- Coulson, C. A.; Eisenberg, D. *Proc. R. Soc. London, Ser. A* **1966**, 291, 445.
- Heggie, M. I.; Latham, C. D.; Maynard, S. C. P.; Jones, R. *Chem. Phys. Lett.* **1996**, 249, 485.
- Batista, E. R.; Xantheas, S. S.; Jonsson, H. *J. Chem. Phys.* **1998**, 109, 4546.
- Silvestrelli, P. L.; Parrinello, M. *Phys. Rev. Lett.* **1999**, 82, 3308.
- Silvestrelli, P. L.; Parrinello, M. *J. Chem. Phys.* **1999**, 111, 3572.
- Sprick, M.; Klein, M. L. *J. Chem. Phys.* **1988**, 89, 7556.
- Ahlström, P.; Wallqvist, A.; Engström, S.; Jönsson, B. *Mol. Phys.* **1989**, 68, 563.
- Zhu, S.-B.; Singh, S.; Robinson, G. W. *J. Chem. Phys.* **1991**, 95, 2791.
- Kozack, R. E.; Jordan, P. C. *J. Chem. Phys.* **1992**, 96, 3120.
- Dang, L. X. *J. Chem. Phys.* **1992**, 97, 2659.
- Cieplak, P.; Kollman, P. A.; Lybrand, T. *J. Chem. Phys.* **1992**, 97, 13841.
- Wallqvist, A.; Berne, B. J. *J. Phys. Chem.* **1993**, 97, 13841.
- Rick, S. W.; Stuart, S. J.; Berne, B. J. *J. Chem. Phys.* **1994**, 101, 6141.
- Chialvo, A. A.; Cummings, P. T. *J. Chem. Phys.* **1996**, 105, 8274.
- Svishchev, I. M.; Kusalick, P. G.; Wang, J.; Boyd, R. J. *J. Chem. Phys.* **1996**, 105, 4742.
- Gao, J.; Pavelites, J. J.; Habibollahzadeh, D. *J. Phys. Chem.* **1996**, 100, 2689.
- York, D. M.; Yang, W. *J. Chem. Phys.* **1996**, 104, 159.
- Liu, Y. P.; Kim, K.; Berne, B. J.; Friesner, R. A.; Rick, S. W. *J. Chem. Phys.* **1998**, 108, 4739.
- Dang, L. X. *J. Phys. Chem. B* **1998**, 102, 620.
- Martin, M. G.; Chen, B.; Siepmann, J. I. *J. Chem. Phys.* **1998**, 108, 3383.
- Sanderson, R. T. *Science* **1951**, 114, 670.
- Parr, R. G.; Donnelly, R. A.; Levy, M.; Palke, W. E. *J. Chem. Phys.* **1978**, 68, 3801.
- Rappé, A. K.; Goddard, W. A., III. *J. Phys. Chem.* **1991**, 95, 3358.
- Kiyohara, K.; Gubbins, K. E.; Panagiotopoulos, A. Z. *Mol. Phys.* **1998**, 94, 803.
- Medeiros, M.; Costas, M. E. *J. Chem. Phys.* **1997**, 107, 2012.
- Chen, B.; Potoff, J. J.; Siepmann, J. I. *J. Phys. Chem. B* **2000**, 104, 2378.
- Grigull, U.; Straub, J.; Schiebener, P. *Steam Table in SI Units*; Springer-Verlag: Berlin, 1984.
- Guissani, Y.; Guillot, B. *J. Chem. Phys.* **1993**, 98, 8221.
- Alejandre, J.; Tildesley, D. J.; Chapela, G. A. *J. Chem. Phys.* **1995**, 102, 4574.
- Errington, J. R.; Panagiotopoulos, A. Z. *J. Phys. Chem. B* **1998**, 102, 7470.
- Badenhoop, J. K.; Weinhold, F. *J. Chem. Phys.* **1997**, 107, 5422.
- Pauling, L. *The Nature of the Chemical Bond*, 3rd ed.; Cornell University Press: Ithaca, 1960.
- Thomas, L. H. *J. Chem. Phys.* **1954**, 22, 1758.
- Miertus, S.; Bartos, J.; Trebatickal, M. *J. Mol. Liq.* **1987**, 33, 139.
- Åqvist, J. *J. Phys. Chem.* **1990**, 94, 8021.
- Åqvist, J. *J. Phys. Chem.* **1991**, 95, 4587.
- Warshel, A.; Weiss, R. M. *J. Am. Chem. Soc.* **1980**, 102, 6218.
- Warshel, A.; Sussman, F.; Hwang, J.-K. *J. Mol. Biol.* **1988**, 201, 139.
- Dixon, M.; Sangster, M. J. L. *J. Phys. C Solid State Phys.* **1976**, 9, L5.
- Chen, B.; Siepmann, J. I. *Theor. Chem. Acc.* **1999**, 103, 87.
- Car, R.; Parrinello, M. *Phys. Rev. Lett.* **1985**, 55, 2471.
- Andersen, H. C. *J. Chem. Phys.* **1980**, 72, 2384.
- Saboungi, M.-L.; Rahman, A.; Halley, J. W.; Blander, M. *J. Chem. Phys.* **1988**, 88, 5818.
- Wilson, M.; Madden, P. A. *J. Phys. Condens. Matter* **1993**, 5, 2687.
- Panagiotopoulos, A. Z. *Mol. Phys.* **1987**, 61, 813.
- Panagiotopoulos, A. Z.; Quirke, N.; Stapleton, M.; Tildesley, D. J. *Mol. Phys.* **1988**, 63, 527.
- Smit, B.; de Smedt, P.; Frenkel, D. *Mol. Phys.* **1989**, 68, 931.
- McDonald, I. R. *Mol. Phys.* **1972**, 23, 41.
- NIST Chemistry WebBook, <http://webbook.nist.gov/chemistry>.
- Odutola, J. A.; Dyke, T. R. *J. Chem. Phys.* **1980**, 72, 5062.
- Dyke, T. R.; Mack, K. M.; Muentner, J. S. *J. Chem. Phys.* **1976**, 66, 498.
- Chialvo, A. A.; Cummings, P. T. *J. Phys. Chem.* **1996**, 100, 1309.
- Soper, A. K.; Turner, J. *Int. J. Mod. Phys. B* **1993**, 7, 3049.
- Soper, A. K.; Bruni, F.; Ricci, M. A. *J. Chem. Phys.* **1997**, 106, 247.
- Báez, L. A.; Clancy, P. *J. Chem. Phys.* **1994**, 101, 9837.
- Bagchi, K.; Balasubramanian, S.; Klein, M. L. *J. Chem. Phys.* **1997**, 107, 8561.
- Jorgensen, W. L.; Jenson, C. *J. Comput. Chem.* **1998**, 19, 1179.

(69) A group-based spherical potential truncation for the electrostatic interactions was used in refs 66 and 68. Thus, these results (in particular, the liquid densities) are not directly comparable with our calculations using the Ewald summation technique. However, the choice of potential truncation might not greatly affect the temperature of maximum density.⁶⁷

(70) Kell, G. S. *J. Chem. Eng. Data* **1975**, 20, 97.

(71) Tsonopoulos, C.; Heidman, J. L. *Fluid Phase Equilib.* **1990**, 57, 261.

(72) Haar, J.; Gallagher, J. S.; Kell, G. S. *NBS/NRC Steam Tables*; Hemisphere: Washington, DC, 1984.